CORPUS PUBLISHERS

Journal of Mineral and Material Science (JMMS)

ISSN: 2833-3616

Volume 5 Issue 4, 2024

Article Information

Received date : September 14, 2024

Published date: October 01, 2024

*Corresponding author

Digby D Macdonald, Department of Nuclear Engineering, University of California at Berkeley, Berkeley, CA 94720, USA

DOI: 10.54026/JMMS/1093

Key Words

Stress Corrosion Cracking; Stainless Steel; Distribution Functions

Research Article

Theoretical Dependencies of the Distributions in Crack Growth Rate in Type ^{304}SS on Various Factors

Jiangbo Shi[1,2], Balazs Fekete[2], Jihui Wang[1], Rajeev K Gupta[3] and Digby D Macdonald[2*]

[1]*School of Materials Science and Engineering, Tianjin University, Tianjin 300072, P R China*

[2]*Department of Nuclear Engineering, University of California at Berkeley, Berkeley, CA 94720, USA*

[3]*Dept of Materials Science & Engineering, North Carolina State University, Raleigh, NC 27606, USA*

Abstract

A purely empirical Artificial Neural Network (ANN) and the high-level deterministic/mechanistic Coupled Environment Fracture Model (CEFM) have been used to study the effects of normal distributions in five independent variables [Electrochemical Potential (ECP), Conductivity (κ), degree of sensitization (EPR), stress intensity factor (K_I), and temperature (T)] on the distribution in the dependent variable (Crack Growth Rate, CGR) for Intergranular Stress Corrosion Cracking (IGSCC) in sensitized Type 304SS in simulated Boiling Water Reactor primary coolant circuits. Both approaches have been useful for gaining a better understanding of the distribution of crack growth rate of stress corrosion cracking in 304SS. We show theoretically that if an independent variable (T, ECP, K_I, EPR, κ) follows a normal distribution (that is, it is randomly distributed), the crack growth rate is commonly lognormally distributed. Finally, the sizes of the Standard Deviations (SDs) in the above variables relative to the means also have a profound impact on the distributions in the dependent variable. If the SDs are small, the distribution in the dependent variable becomes indistinguishable from a normal distribution. However, if the SDs are large, the distribution in the dependent variable is unequivocally lognormal.

Introduction

In the early 1970s, numerous cases of Intergranular Stress Corrosion Cracking (IGSCC) occurred in sensitized AISI Type 304 austenitic stainless steels in Boiling Water Reactors (BWR) [1]. The root cause for this cracking is a combination of tensile stress, an oxidizing environment from the radiolysis of water producing a molar excess of oxygen (O_2) and hydrogen peroxide (H_2O_2) over hydrogen (H_2), which is preferentially stripped from the coolant by boiling in the reactor core, and a sensitized microstructure. Stress Corrosion Cracking (SCC) continues to be a safety concern in Light Water Reactor (LWR) operation. The SCC mechanism involves complex interactions between metallurgy, mechanical (stress), and external environmental factors. For these reasons, assessing and predicting failures of in-vessel Stainless Steel (SS) components in BWRs from intergranular SCC (IGSCC) is difficult. Furthermore, the uncertainty in the input data (i.e., in the independent variables) makes the prediction of SCC with engineering accuracy especially challenging.

Structural components in nuclear power plant are designed to resist different types of loading, such as static loads, operating pressure, thermal loads, and other transient loads. Damage due to SCC and IGSCC occurs in a susceptible material, in a corrosive environment, and in the presence of high temperature and high applied and residual stresses. Because the operating and environmental conditions vary considerably during the lifetime of the power plant, the life of the structural components against SCC must be assessed in a probabilistic sense. However, this is further hampered by not currently knowing unequivocally the relationships between the distributions in the independent and dependent variables in the system.

Several studies have assessed the probabilities of failure indifferent components in operating power plants and oil and gas pipelines. Swati Jain et al. [2,3] used Bayesian networks to predict the probability of high-pH SCC failure in pipelines and discussed the effects of stress and other factors that affect high-pH SCC. They demonstrated that the model can be used to assess the probability of failure due to SCC at different times for different pipeline segments. Priya et al. [4] computed the failure probabilities of a piping component against SCC with time using Monte Carlo simulation techniques, they took the degree of sensitization, applied stress, time to initiation of SCC, initial crack length, and initiation crack growth velocity as randomly distributed independent variables. The simulation results were found to be in satisfactory agreement with the relevant experimental observations from the literature. Through characterizing Intergranular Stress Corrosion Cracking (IGSCC) using a single damage parameter and using the general methodology recommended in the modified computer program Piping Reliability Analysis Including Seismic Events, Guedri [5] assessed the IGSCC of stainless-steel piping in a probabilistic manner. Anoop [6] computed the fuzzy failure probabilities of a piping component against SCC with time using an approach combining the vertex method with the Monte Carlo simulation technique. Based on the source and type of uncertainty, the relevant variables were treated as random or fuzzy, to consider the uncertainty of those variables.

From the results obtained, it is noted that the fuzzy-probabilistic approach presented shows promise for safety assessment of nuclear power plant pipelines. Andresen & Ford [7] proposed the slip dissolution/film rupture model to predict the observed crack growth rates for the stainless steels, nickel alloys, and low-alloy steels in high temperature water (reactor coolant) systems. It was demonstrated that ranges in the distributions are easily input into the model, and a variety of approaches can be used for statistical and probabilistic treatment. Finally, Macdonald and Urquidi-Macdonald [8-11] developed the Coupled Environment Fracture Model (CEFM), which combines the electrochemistry and the mechanics of the system to predict the Crack Growth Rate (CGR) in a highly deterministic manner and showed that the predicted CGR is at least as accurate as that measured in the laboratory ($\pm 0.2\log_{10}$ units) in many cases. This level of accuracy was demonstrated by training an Artificial Neural Network (ANN) on a large database of dependent variable (CGR) vs independent variable (T, ECP, K_I, EPR, κ) relationships gleaned from the literature [12,13].

In this paper, we explore the distribution in CGR for a piping component made of Type 304 stainless steel in BWR primary coolant (pure water at 288 °C), because this type of steel is highly susceptible to IGSCC. Based on the models that we have developed previously to predict the crack growth rate in sensitized Type 304SS and other alloys in aqueous environments, including high temperature water systems [8-22], as a function of the degree of sensitization, conductivity, pH, electrochemical potential, stress intensity factor. and temperature. In this study, these independent variables are randomly distributed about means with the distributions being normal. Then, we studied the effect of each variable on the distribution in crack growth rate of Type 304SS under different environmental conditions.

The objectives of the present work are to explore the probabilistic natures of both a theoretical, mechanism-based model for crack advance {the Coupled Environment Fracture Model (CEFM) [12,13]} and an Artificial Neural Network (ANN) [9-11] that contains no theoretical basis (i.e., contains no physico-chemical model or mechanism but is purely empirical in nature) and to determine if the two approaches yield similar results. This is done by distributing each independent variable (T, ECP, K_I, etc.) normally about a mean with an assigned standard deviation and enquiring into the nature of the distribution in the dependent variable (crack growth rate, CGR).

Modeling of Stress Corrosion Cracking

Coupled environment fracture model (CEFM)

As a deterministic, physico-electrochemical model for predicting crack growth rate, the Coupled Environment Fracture Model (CEFM) is used here to account for the effect of variations of input variables on the crack growth rate. In this section, we briefly review the CEFM, so that the reader may appreciate its theoretical underpinnings. Since its inception in 1991 [8,9], the CEFM has been used extensively and successfully to model crack growth rate in sensitized Type 304SS in Boiling Water Reactor (BWR) primary coolant environments and in dilute sulfate solutions over the temperature range of 50-300 °C. The CEFM code has been modified and calibrated to predict crack growth rate in aluminum marine alloys (e.g. AA 5083) in NaCl brine [14], in ASTM A470/471 turbine disk steels in simulated steam condensate [15], in Alloy 22 in simulated Yucca Mountain surface deliquescent environments [16], in Alloy 600 in prototypical PWR primary coolant [17], and has been recently used to account for the evolution of semi-elliptical surface cracks [15]. Of particular importance is the ANN analysis of the empirical CGR data for Type 304SS [12] and Alloy 600 [13], because that defined the "character" of IGSCC in these alloys by establishing relationships between the dependent variable (CGR) and the various independent variables (T, K_I, yield strength, ECP, etc). The CEFM was found to accurately account for the IGSCC character of the cracks [12,13].

The physic-electrochemical basis of the CEFM is the differential aeration hypothesis (DAH), as shown in Figure 1.

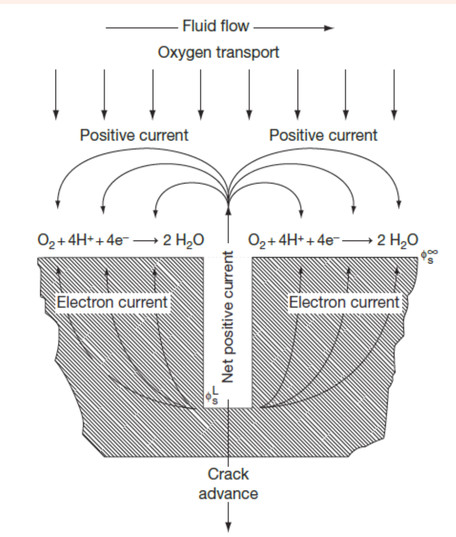

Figure 1: Schematic of the differential aeration hypothesis for localized corrosion as incorporated in the CEFM.

In this model, crack advance is assumed to occur via the slip/dissolution/ repassivation mechanism augmented with Hydrogen-Induced Cracking (HIC), with the governing equation being a statement of charge conservation that is expressed as follows:

$$i_{crack}A_{crackmouth} + \int_S i_C^N ds = 0 \quad \text{(1a)}$$

or equivalently

$$\int_S i^N ds' = 0 \quad \text{(1b)}$$

(both have been used in various versions of the model), where i_{crack} is the net (positive) current density flowing from the crack mouth, $A_{crack\cdot mouth}$ is the crack mouth area, i_C^N is the net (cathodic) current density due to charge transfer reactions on the external surface, i^N is the net current density, and ds and ds' are areal increments on the external surface and on the entire area (including the area inside the crack), respectively. The subscript s on the integral indicates that the integration is to be performed over the areas just defined.

The CEFM model performs its calculation in two steps [8,9]. Firstly, it calculates the electrochemical potential of the external surface (E_{corr}) and secondly the crack growth rate is estimated. The electrochemical potential sufficiently far from the crack is calculated using the mixed potential model from the composition and properties of the system [19], such that the local electrochemical properties are unaffected by the presence of the crack, and, hence, that the potential in the solution with respect to the metal is equal to the negative of the free corrosion potential (the ECP). This condition holds for distances of a few tens of Crack Mouth Opening Displacements (CMODs) on either side of the crack center line, as determined by the conductivity of the environment and as determined by numerical simulation [8,9]. The crack growth rate calculation depends on splitting the crack environment into the crack-internal and the crack-external environments and by noting that the transport (Nernst-Planck) and potential distribution (Poisson's or Laplace's) equations for both environments are coupled by common boundary conditions (concentrations and electrostatic potential) at the crack mouth. To solve the crack growth rate, an electrochemical potential at the crack mouth (the boundary between the crack-internal and - external environments) is assumed and the transport equations for the crack internal and external environment are solved. It is generally found that Equations (1) or (2) are not satisfied. The value of the crack mouth potential is then changed iteratively until the current in the crack-internal and crack-external match and hence Equations (1) or (2) are satisfied. For each iteration of this calculation on the internal and external currents, an electrochemical potential is initially assumed at the crack tip and this value is changed iteratively within an embedded loop until the electro-neutrality condition is satisfied at the crack tip within each iteration of the crack mouth potential.

The calculation is repeated iteratively on the crack mouth potential until charge is found to be conserved. The crack internal current is then obtained by solving the Nernst-Planck equations for each of the ten species in the system [H^+, Fe^{2+}, $Fe(OH)^+$, Ni^{2+}, $Ni(OH)^+$, Cr^{3+}, $Cr(OH)_2^+$, Na^+, Cl^-, OH^-], with the appropriate boundary conditions of $C_i^{mouth} = C_i^b$, i = 1, 10, where C_i^{mouth} and C_i^b are the species concentrations at the crack mouth and in the bulk solution, respectively, recognizing that the source of the current is alloy dissolution at the crack tip as described by the slip/dissolution/ repassivation mechanism [8,9]. For Fe^{2+}, $Fe(OH)^+$, Ni^{2+}, $Ni(OH)^+$, Cr^{3+}, $Cr(OH)_2^+$, $C_i^b = 0$, but for H^+, OH^-, Na^+, and Cl^- the bulk concentrations are finite, depending upon the composition of the solution, with $C_{H^+}^b C_{OH^-}^b = K_W C_{H^+}^b C_{OH^-}^b = K_W$. The boundary conditions for each specie at the crack tip is expressed in terms of the kinetics of dissolution of each component of the alloy recognizing that electroneutrality must hold; i.e., $\sum_{i=1}^{10} Z_i C_i^{tip} = 0 \sum_{i=1}^{10} Z_i C_i^{tip} = 0$, where $C_i^{tip} C_i^{tip}$ is the concentration of species i at the crack tip. Note, that the potentials are defined as electrostatic potential in the solution with respect to the metal, which is assumed to be an equipotential phase. Accordingly, the potential at the surface remote from the crack mouth is simple $-E_{corr}$ and that at the crack tip is $-E_{tip}$. For the calculation of the external current, a 40-term Fourier series solution to Laplace's equation is employed, as described elsewhere [8]. Importantly, measurement of the coupling current and the noise contained therein [20] demonstrates that the micro-fracture frequency is much too low and the micro-fracture dimension is much too large to be attributed to classical slip-dissolution-repassivation and that the crack growth rate is partly determined by Hydrogen-Induced Cracking (HIC), probably via the formation of strain-induced martensite on the grain boundaries ahead of the crack tip into which hydrogen is injected from the crack tip where residual hydrogen evolution occurs. The larger micro-fracture dimensions have been confirmed by analyzing the noise in the coupling current due to IGSCC in sensitized Type 304 SS in thiosulfate-containing solutions [21,22] and fracture in AISI 4340 steel in NaOH solutions [23] both being recognized as classical HIC systems. Finally, we note that a fully analytical form of the CEFM has been developed with the important advantage of computational speed [24].

Artificial neural network model

As non-deterministic, empirical models, Artificial Neural Networks (ANNs) have non-linear mapping structures that can be applied for predictive modeling and classification. They are inspired by the structure of the cerebral cortex portion of the brain, where billions of neurons (in humans and in higher-order animals) are interconnected to process a variety of complex information. An artificial neural network consists of data processing "neurons" joined in layers. Typically, there is an input layer through which the data are presented to the network and an output layer where the network response is obtained. Between these two layers, there exist one or more layers of neurons called "hidden layers". The strength of the interconnections between a neuron in any given layer with all the neurons in neighboring layers, to which it is connected, is determined by the weight and bias associated with them. Establishment of the noon-volatile weights essentially imbues the net with "memory" and enables the relationships between the output (in our case the CGR) and each of the independent input variables [T, ECP, Conductivity, K_I, and Degree of Sensitization of the steel (EPR)] to be defined. For more details about the training and prediction of crack growth rate in Alloy 600 and Type 304SS in high temperature reactor coolant using ANNs, please see [12,13].

Results and Discussion

In this study, the stochastic distributions in crack growth rate due to SCC in sensitized Type 304SS is simulated using both the CEFM and the ANN model. This is done by randomly distributing the chosen independent variable (X) around a mean $(\bar{X})$ $(\bar{X})$ with a standard deviation (σ_X):

$$\frac{dN}{dX} = \frac{1}{\sigma\sqrt{2\pi}} e^{\frac{-(X-\bar{X})^2}{2\sigma_X^2}} \qquad (1)$$

The default values of the random variables together with the assumed standard deviations considered in this study are given in Table 1. When we study the effect of the variation of one independent variable on the CGR, all the other independent variables are assigned their undistributed default values (Table 1), while values for the variable under investigation are randomly chosen, using a random number generator, from a database that contains 1000 data points spread over the range $\bar{X} \pm 3\sigma_X \bar{X} \pm 3\sigma_X$. This range corresponds to a 99.7 % probability that a future measurement of X will fall within that range.

Table 1: Summary of the random variables considered in this study.

Variable	Distribution	Mean Value	Standard Deviation
ECP (V_{SHE})	Normal	0.1	0.05
Conductivity (μs/cm)	Normal	2.6	0.13
Temperature (ºC)	Normal	288	5
Stress intensity factor (MPa·√m)	Normal	30	5
Degree of sensitization (C/cm²)	Normal	15	5

A principal finding of this study is that while an independent variable (T, ECP, K_I, DoS, conductivity, etc) may be distributed normally, reflecting a stochastic input, the dependent variable (CGR) is commonly lognormally distributed provided that the standard deviation is sufficiently large, as indicated by analysis of data obtained from the theoretical model (CEFM) and from the experimental data in the literature via the ANN. If the standard deviation is small, the distribution, although being fundamentally lognormal in nature, mimics a normal distribution. A lognormal distribution is a continuous probability distribution of a random variable whose logarithm is normally distributed. Thus, if the random variable, X, is log-normally distributed, then the dependent variable displays a normal distribution and vice versa. As seen below, in many instances, the logarithm of the dependent variable (the CGR) depends linearly on the independent variable, within uncertainty in the data. For example, within the region of ECP where the CGR is dominated by the electrochemistry (ECP > -0.23 V_{she}), log(CGR) varies linearly with ECP [10]. Accordingly, the dependent variable, Y (CGR), can be written as:

$$Y = exp(aX) \qquad (2)$$

where a is a constant and X is the independent variable. Thus, from distribution theory, if is X is normally distributed, as assumed in this study, then the dependent variable (Y) must be lognormally distribution. We show below that this expectation is fulfilled. The probability density function for a log normal distribution is given mathematically as:

$$\frac{dN}{dY} = \frac{1}{X\sigma\sqrt{2\pi}} exp\left[-\frac{(Y-\mu)^2}{2\sigma^2}\right] \qquad (1)$$

where the mean is exp($\mu+\sigma^2/2$), median is exp(μ), Mode is exp($\mu-\sigma^2$), and the variance is [exp(σ^2-1)]exp($2\mu+\sigma^2$). The mode corresponds to the maximum in the distribution; that is to the value of the independent value that has maximum probability.

Impact of ECP on the distribution in CGR

Histograms of the calculated CGR as a function of ECP are shown in Figure 2. The values for all the other input parameters are as given in Table 1. The log-normal fitted lines are also shown in the figure. As can be seen from this figure, with the increase of ECP the CGR increases accordingly. Note that the lognormal distribution moves to the right with increasing ECP, in the direction of increasing CGR, with the standard deviation also increasing, making the distributions wider, even though a fixed standard deviation (0.05 V, Table 1) was assumed in the normal distribution in ECP. This indicates that if the input parameters are randomly distributed around a certain value, the calculated CGR will also have stochastic character, which approximates to a lognormal distribution.

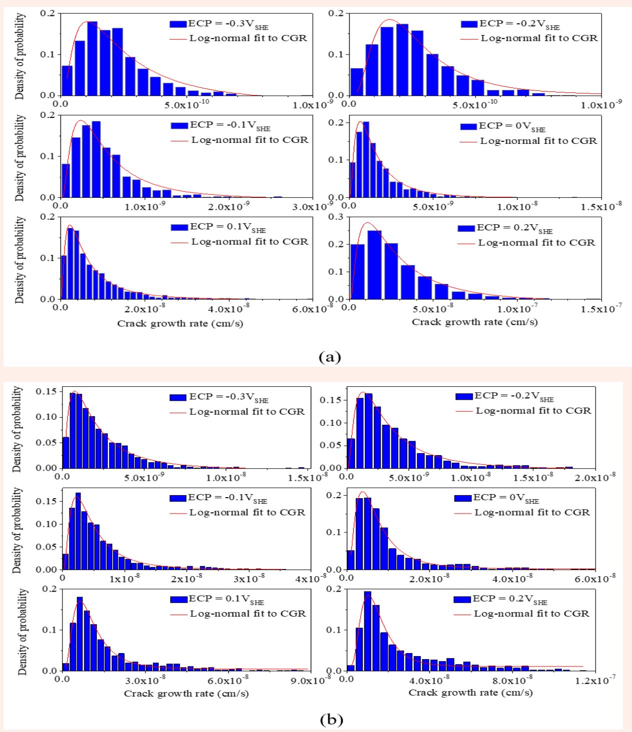

Figure 2: Histograms of the calculated CGRs under different ECP compared to the fitted log-normal distributions. (a) Results from the CEFM; (b) Results from the ANN model.

Figure 3 shows the dependence of the mean value of CGR on ECP, as determined by both the CEFM and the ANN. It is evident that the CEFM predicts that the crack growth rate is significantly higher than obtained by training an ANN of experimental data in the literature. This discrepancy is traced to the paucity of CGR data at low ECP upon which the net is trained. Such data are extraordinarily difficult to obtain using current techniques (e.g., reverse potential drop or compliance methods for measuring crack length as a function of time), because the values are low (of the order of 1-2x10^{-10}

cm/s). As shown by the CEFM, the CGR tends toward a value that is independent of ECP as ECP becomes increasingly more negative (ECP < -0.3 V_{SHE}), corresponding to the mechanical creep limit. The ANN was not trained on data that contained this limit and it is for that reason that no creep limit is predicted by the net.

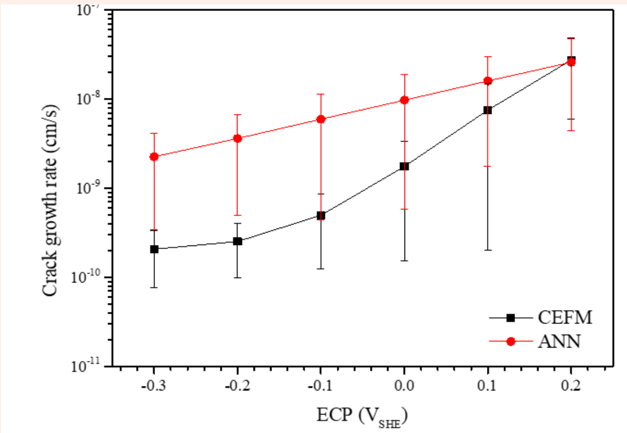

Figure 3: Dependence of the mean value of CGR on ECP calculated using both the CEFM and ANN model.

Both the CEFM and the ANN predict that the CGR increases exponentially with increasing ECP when ECP > -0.23 V_{she}. Furthermore, the CEFM predicts the well-known, expected sigmoid relationship between the CGR versus ECP, because the CGR tends toward an upper, mass transfer limit that is not a strong function of potential [10]. Again, note that the CEFM predicts the creep rate for 304SS, when the ECP is lower than -0.3 V_{SHE}, however, there is no such trend for ANN model. As noted above, this is because the CGR is so small at lower ECP that it was never included in the experimental database upon which the ANN was trained. Accordingly, the predicted CGRs from the ANN at lower ECP are much higher than that calculated from the CEFM model, but this is an artifact of the CGR database not including data at or close to the creep CGR limit. However, as the ECP increases, the predicted results from both the CEFM and the ANN come into better agreement, as electrochemical effects become increasingly dominant over creep.

Impact of stress intensity factor on the distribution in CGR

Histograms of the calculated CGR for different K_I values are shown in Figure 4. These curves were generated assuming a standard deviation in K_I of 5 MPa.m$^{1/2}$ (Table 1). All the other input parameters have their default values as is also shown in Table 1. The log-normal distribution provides an adequate description of the CGR distributions, as can be seen in Figure 4. For the predicted results from the CEFM, as shown in Figure 4(a), the lognormal distribution moves a little to the right as K_I increase from 20 Mpa·√m to 30 Mpa·√m, meanwhile, when K_I is above 30 Mpa·√m, there is almost no effect of K_I on the CGR. However, for the results obtained from the ANN, with the increasing KI, the CGR increases gradually. As indicated in Figure 4(b) the peak value of the log-normal fitted curve moves to the right, combined with an increase of the standard deviation, making the distribution wider. The mean value and the standard deviation of the CGR calculated from both the CEFM and the ANN are shown in Figure 5.

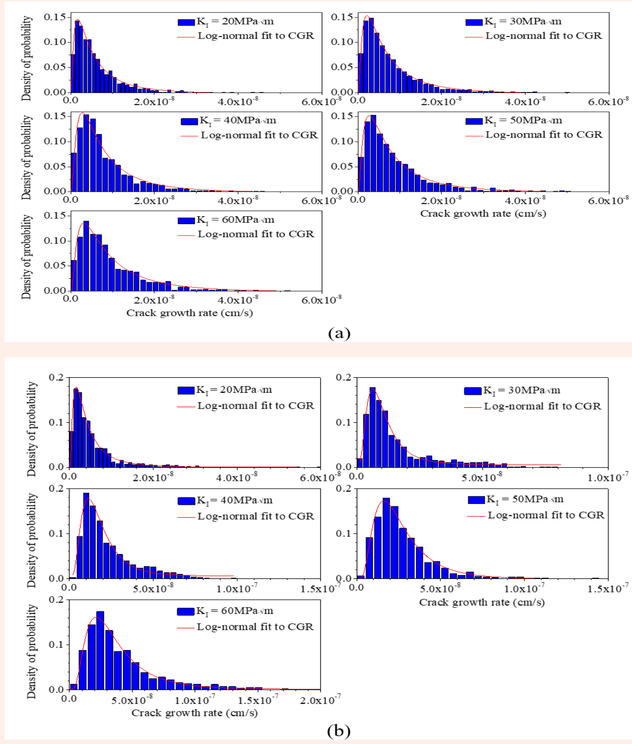

Figure 4: Histograms of the calculated CGRs under different KI compared to the fitted log-normal distributions. (a) Results from the CEFM; (b) Results from the ANN.

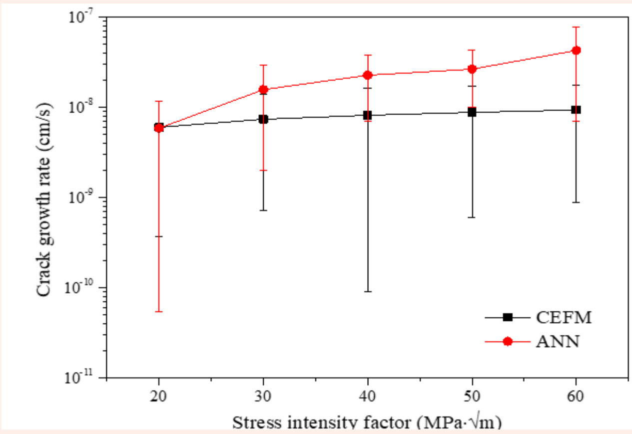

Figure 5: Dependence of the mean value of CGR on K_I calculated using both the CEFM and ANN model.

As depicted above, the ANN predicts that the CGR increases with increasing K_I; however, the results from the CEFM show little effect of K_I on the CGR. Because the error bars overlap, it is evident that the CEFM predicted results and those predicted by the ANN are in good agreement, in general. The reason for the weak dependence of the CGR on K_I is that the system is in the Stage II region of the CGR/K_I correlation, where the CGR is dominated by electrochemical, rather than mechanical factors. Accordingly, no strong dependence was expected.

Impact of temperature on the distribution in CGR

Figure 6(a-b) shows the histogram of the effect of temperature on the CGR. All the other input parameters are as shown in Table 1. The standard deviation assumed in the normal distribution in T is 5 ºC (Table 1). As can be seen from Figures 6(a) & 6(b), there is little effect of temperature on the CGR over the range explored (200 to 300 ºC); as the temperature increases, the tail of the distribution of CGR moves slightly to the left. Elsewhere, it is shown via experiment [24] and the CEFM [10] that the CGR passes through a maximum at about 200 ºC. However, in those studies, all the independent variables varied with temperature, whereas in the present study, they are assigned the fixed, default values that are listed in Table 1. Vankeerberghen & Macdonald [11-13] argued that the effect of temperature on CGR in Type 304 reflects a competition between the positive impact on the rate of the cathodic depolarizer reaction on the surfaces external to the crack together with the positive impact on the crack tip strain rate and the observed negative impact on the corrosion potential, such that the former dominate at T < 200 ºC but the latter dominates at T > 200 ºC. In the present case, there is little effect of temperature on the CGR (Figure 7); this is because the CGR in this paper was calculated assuming that all the other independent variables and parameters (e.g., ECP, conductivity, pH, crack tip strain at fracture) have constant values. The CEFM and the ANN allow us to study the effect of each variable on the CGR independently. The lognormal distributions, as shown in Figure 6, give a good description of the scattered CGR. Finally, good agreement is obtained for the CGR predicted from both the CEFM and the ANN [25].

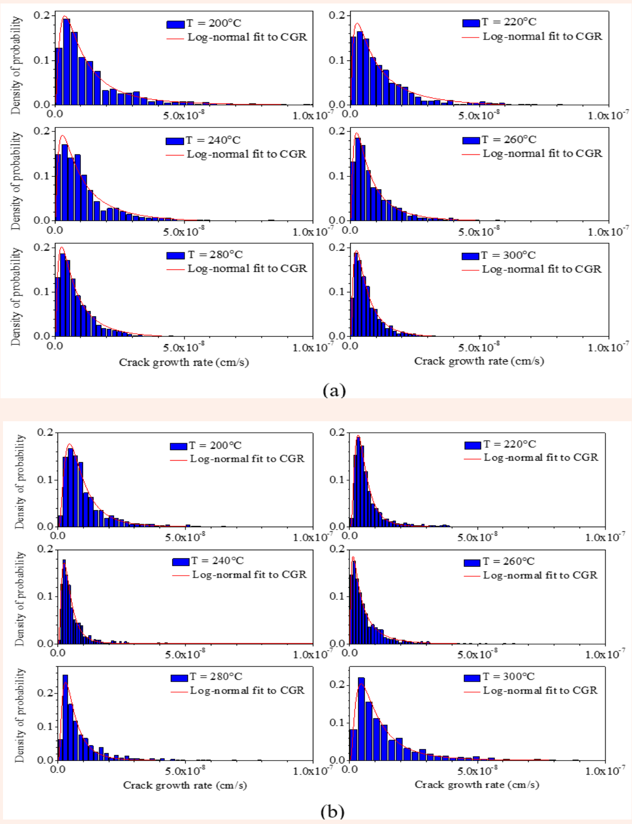

Figure 6: Histograms of the calculated CGRs under different temperature compared to the fitted log-normal distributions. (a) Results from the CEFM; (b) Results from the ANN.

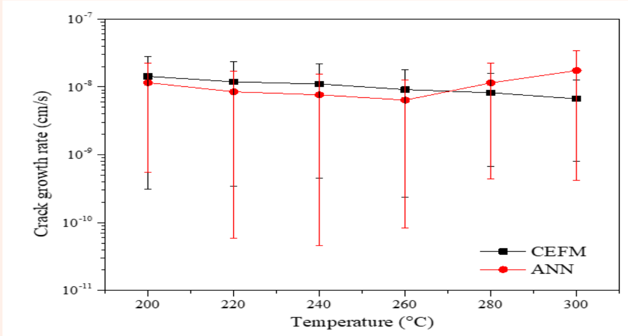

Figure 7: Dependence of the mean value of CGR on temperature calculated using both the CEFM and ANN.

Impact of conductivity on the distribution in CGR

According to the CEFM [8-10,26] the principal effect of increasing conductivity is to increase the throwing power of the current from the crack mouth, such that a larger area on the external surface may contribute to the annihilation of the coupling current via the redox reactions that occur on the external surface (e.g., oxygen reduction). Accordingly, the coupling current increases and, because the CRG is linearly related to the coupling current via Faraday's law, the CGR increases correspondingly. Figures 8(a) & 8(b) show the histograms of CGR as a function of conductivity. As can be seen from Figures 8(a) & 8(b), as the conductivity increase from 2.6 µs/cm to 3.4 µs/cm, the CGR distribution moves to the right; this phenomenon is more apparent from the results predicted by the ANN. The fitted lognormal distribution lines are also shown in Figure 8, which gives an adequate description of the CGR distributions. Figure 9 shows the dependence of mean CGR on conductivity. The CEFM predicts there is almost no effect of conductivity on CGR over the limited range considered in these calculations (between 2.6 µs/cm to 3.4 µs/cm), while the ANN predicts a small increase in CGR with increasing conductivity. In general, the results calculated from both the CEFM, and the ANN agree well.

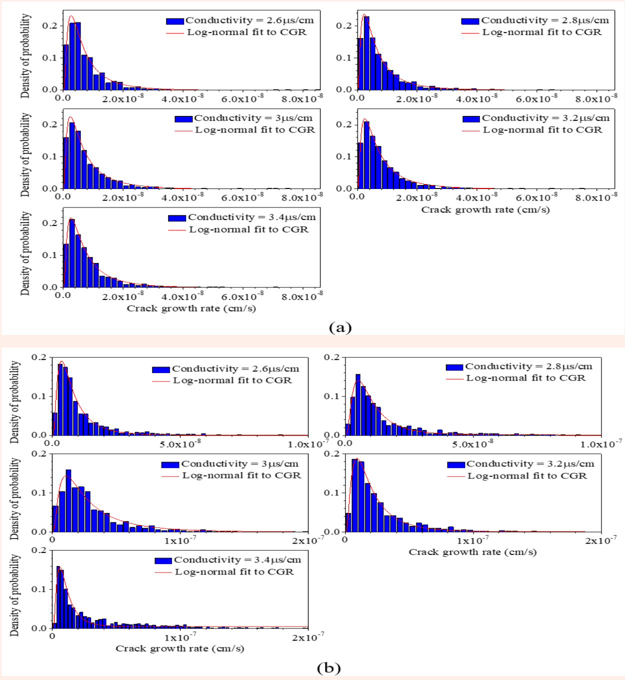

Figure 8: Histograms of the calculated CGRs under different conductivity compared to the fitted log-normal distributions. (a) Results from the CEFM; (b) Results from the ANN.

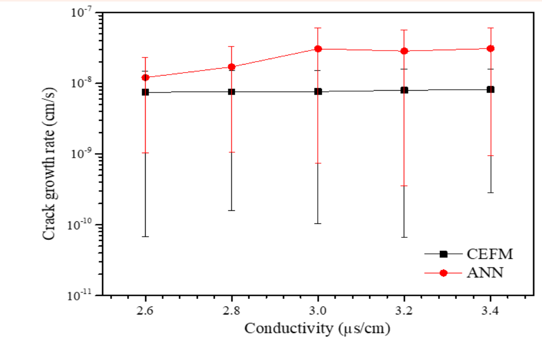

Figure 9: Dependence of the mean value of CGR on conductivity calculated using both the CEFM and ANN.

Impact of the degree of sensitization on the distribution in CGR

The intergranular cracking susceptibility of Type 304SS in high-temperature water is known empirically to be a function of the degree of grain boundary sensitization. (i.e., the extent of chromium depletion in the matrix adjacent to grain-boundary due to $Cr_{23}C_6$ precipitation on the boundary) [1,7,10,19]. The degree of sensitization, DoS, is commonly determined using the double loop, electrochemical potentio-kinetic reaction method, DL-EPR, and is expressed as an "EPR" or "DoS" number with units of C/cm^2. In a previous paper [12], based on the predictions of the ANN, we proposed a calibration equation to account for the effect of sensitization on CGR in the CEFM model. Here we use both the ANN and the CEFM to study the distribution characteristics of the CGR when all other independent variables (K_I, T, Conductivity, EPR, and ECP) obey normal distributions with a preselected means standard deviation. Figure 9(a-b) show the histograms of CGR under different EPR.

As can be seen from Figures 10(a) & 10(b), the distribution of CGR mainly concentrates on the left side of the graph when the EPR is 10 C/cm^2, however, as the EPR increases to 20 C/cm^2 the distribution of CGR moves to the right, and it becomes wider, which means the standard deviation increases with the increase of CGR. The lognormal distribution fitted lines are also shown in Figures 10(a) & 10(b) and provide an adequate description of the distributions in the CGR. The dependence of the mean CGR on EPR is shown in Figure 11. An increase of CGR with increasing EPR can be seen from Figure 11, which agrees well with other findings [12,13].

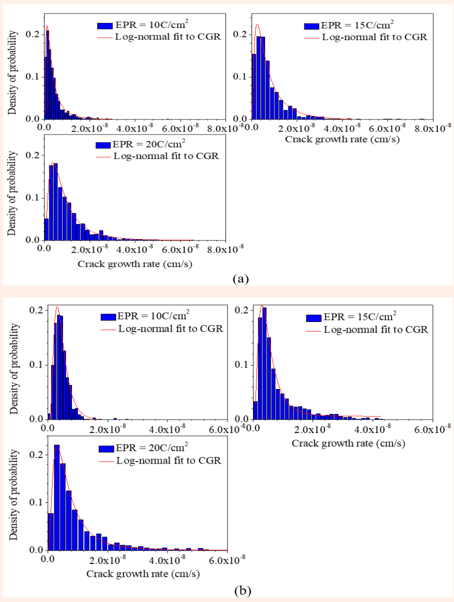

Figure 10: Histograms of the calculated CGRs under different EPR compared to the fitted log-normal distributions. (a) Results from the CEFM; (b) Results from the ANN.

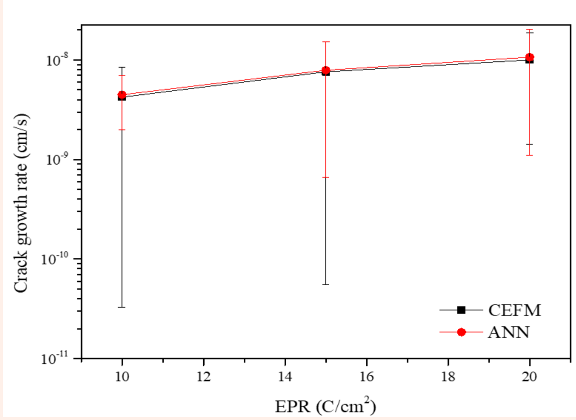

Figure 11: Dependence of the mean value of CGR on DOS calculated using both the CEFM and the ANN.

Impact of standard deviation magnitude

Standard deviation in ECP: The studies reported above assumed preselected values of the standard deviations of the normal distributions in the independent variables as summarized in Table 1. While those standard deviations were chosen to be realistic of what might be experienced in service, it is important to explore the impact of the magnitudes of the standard deviations on the normal distributions of the independent variables on the distributions in the dependent variable (CGR). The standard deviation of ECP has an obvious effect on the distribution type of CGR, as can be seen from Figure 12 & Table 2. Thus, when the standard deviation in ECP is less than 0.01 V_{she}, the CGR obeys a normal distribution; however, as the standard deviation increases to more than 0.03V_{she}, the distribution in CGR changes to lognormal as displayed in Figure 2.

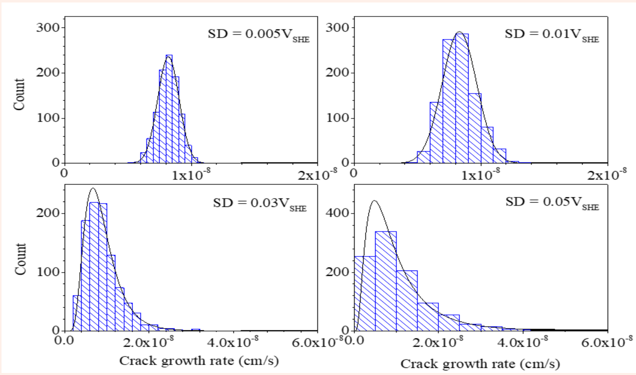

Figure 12: Histogram of crack growth rate under different ECP standard deviation.

Table 2: Statistical results of CGR under different ECP standard deviation.

ECP(V_{SHE})	Crack Growth Rate (cm/s)		P-Value	Distribution
Standard Deviation	s	m		
0.005	$8.44x10^{-10}$	$8.19x10^{-9}$	0.894	Normal
0.01	$1.37x10^{-9}$	$8.30x10^{-9}$	0.085	Normal
0.03	$4.16x10^{-9}$	$8.97x10^{-9}$	0.861	Log-normal
0.05	$7.73x10^{-9}$	$1.00x10^{-8}$	0.301	Log-normal

Noting that the mean value of conductivity is 3uS/cm, the variation of its standard deviation has little effect on the distribution type of CGR. All the CGR obey normal distribution under different values for the standard deviation in solution conductivity.

Standard deviation in the stress intensity factor: Figures 6-3 shows the distribution of crack growth rates under different standard deviation ranges when the stress intensity factor is 30MPa·√m. It can be seen from Figure 6-3 that when the standard deviation of K_I increases from 1MPa·√m to 4MPa·√m, the distribution of crack growth rate does not change, and its distribution range does not change. After KS hypothesis test, it can be concluded that the crack growth rate in different standard deviation ranges follows a normal distribution. Comparing the results in Figure 4-9, it can be concluded that when the value of K_I is greater than 9MPa·√m, the increase of K_I basically has no effect on the crack growth rate. In this case, K_I is not a controlling factor for the development of crack growth rate (Other factors such as corrosion potential may be the controlling factor). As can be seen from Figure 13 & Table 3, the variation in the standard deviation in K_I has little effect on the distribution type of CGR. All the CGR distributions are normal under the different standard deviations in K_I.

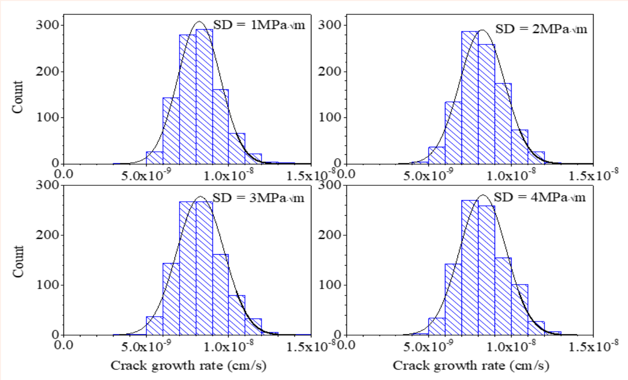

Figure 13: Histogram of crack growth rate under different K_I standard deviation'.

Table 3: Statistical results of CGR under different K_I standard deviation and Kolmogorov-Smirnov (K-S) test results.

K_I (MPa·√m)	Crack Growth Rate (cm/s)		P-Value	Distribution
Standard Deviation	s	m		
1	$1.29x10^{-9}$	$8.2x10^{-9}$	0.063	Normal
2	$1.37x10^{-9}$	$8.23x10^{-9}$	0.201	Normal
3	$1.44x10^{-9}$	$8.29x10^{-9}$	0.05	Normal
4	$1.42x10^{-9}$	$8.28x10^{-9}$	0.052	Normal

Standard deviation in the temperature: As can be seen from Figure 14, under four different standard deviation values of temperature, the CGR obeys the normal distribution function. There is no effect of variation of standard deviation on the CGR distribution type (Table 4).

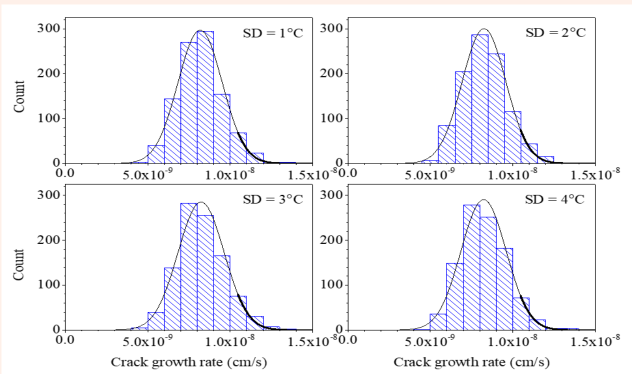

Figure 14: Histogram of crack growth rate under different temperature standard deviation.

Table 4: Statistical results of CGR under different temperature standard deviation.

Temperature (°C)	Crack Growth Rate (cm/s)		P-Value	Distribution
Standard Deviation	s	m		
1	$1.34x10^{-9}$	$8.18x10^{-9}$	0.292	Normal
2	$1.33x10^{-9}$	$8.26x10^{-9}$	0.205	Normal
3	$1.4x10^{-9}$	$8.24x10^{-9}$	0.132	Normal
4	$1.37x10^{-9}$	$8.23x10^{-9}$	0.07	Normal

Standard deviation in the degree of sensitization: There is no effect of variation of standard deviation of DoS on the CGR distribution type. All the CGR data obey normal distributions (Figure 15), and the statistical results are shown in Table 5.

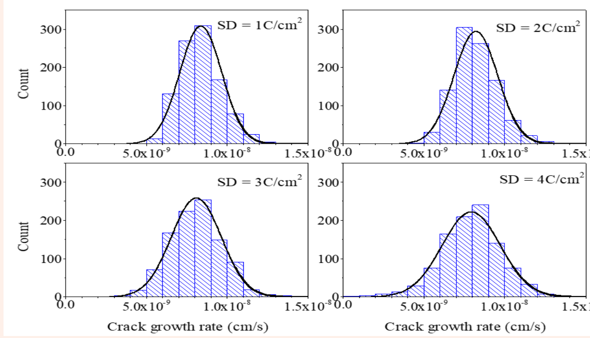

Figure 15: Histogram of crack growth rate under different EPR standard deviation.

Table 5: Statistical results of CGR under different EPR standard deviation.

EPR (C/cm²)	Crack Growth Rate (cm/s)		P-Value	Distribution
Standard Deviation	s	m		
1	$1.29x10^{-9}$	$8.35x10^{-9}$	0.05	Normal
2	$1.35x10^{-9}$	$8.2x10^{-9}$	0.051	Normal
3	$1.54x10^{-9}$	$8.1x10^{-9}$	0.932	Normal
4	$1.8x10^{-9}$	$7.9x10^{-9}$	0.149	Normal

Standard deviation in the solution conductivity: Figure 16 shows the distribution histogram of the crack growth rate under different standard deviations when the solution conductivity is 3 μS/cm. Other input parameters are shown in Table 6. It can be seen from the figure that when the solution conductivity is 3 μS/cm, the change of its standard deviation does not affect the distribution of the crack growth rate, and the distribution of the corresponding crack growth rate obeys the normal distribution. The corresponding statistical results are shown in Table 6 also confirms this. This result shows that, although the conductivity of the solution plays an important role in the stress corrosion cracking process, under the test conditions assumed in this chapter, the conductivity of the solution is no longer the limiting factor affecting the crack growth rate (3 μS/cm is already large enough), Other factors such as quality transmission process may be limiting steps.

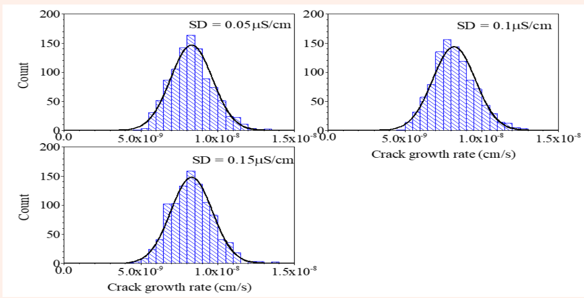

Figure 16: Histograms of crack growth rate for different conductivity standard deviations.

Table 6: Statistical results of CGR for different conductivity standard deviations.

Conductivity (μS/cm)	Crack Growth Rate (cm/s)		P-Value	Distribution
Standard Deviation	s	μ		
0.05	$1.36x10^{-9}$	$8.30x10^{-9}$	0.059	Normal
0.1	$1.39x10^{-9}$	$8.20x10^{-9}$	0.052	Normal
0.15	$1.35x10^{-9}$	$8.30x10^{-9}$	0.57	Normal

Other independent variables exist in the system that might also be distributed in exploring their impact on the distribution of the dependent variable (CGR). For example, Kwon et al. [27] demonstrated that flow velocity can have a profound impact on the CGR in Type 304 SS in simulated BWR primary coolant [28,29]. For low aspect ratio cracks (AR < 5), increasing flow rate inhibits CGR, consistent with the washing out of the crack enclave and discouraging the establishment of the aggressive conditions via differential aeration that are necessary (low pH, high [Cl^-]) to maintain an active crack [30]. The effect is consistent with a counter-rotating cell model for the exponential decrease in the intensity of mixing as one moves from the crack mouth towards the crack tip. This effect may also be interpreted as a mixing-induced decrease in the electrochemical crack length due to the external environment increasingly penetrating the crack enclave as the flow velocity in the external environment increases. On the other hand, the CGR of high aspect ratio cracks (AR > 5) is accelerated with increasing flow velocity, which is attributed to enhanced mass transfer of oxygen to the external surface that shifts the ECP in the positive direction resulting in the observed increase in the CGR [30]. Thus, inhibition of CGR at low aspect ratios is expected to impact crack initiation and the "short crack" problem whereas enhancement of the CGR will have its greatest impact on deep, well-established cracks.

Summary and Conclusions

CGR in Type 304SS in high temperature water systems has been modelled using the CEFM model and the ANN model. Five common independent variables (K_I, T, Conductivity, EPR, and ECP) were chosen as input parameters to these two models. All the input parameters were assigned a normal distribution characteristic and the distribution characteristic of CGR under different conditions were studied. Both the CEFM model and the ANN model account for the variables dependence of the CGR, and good agreement between the results from these two models have been obtained. Given that the input parameters obey normal distribution, the CGR distribution approximates to a log-normal distribution.

Conclusion

The CEFM is used to study the influence of random errors of different independent variables (temperature, corrosion potential, solution conductivity, sensitization, stress intensity factor and pH) on the crack growth rate distribution in the stress corrosion cracking of 304 stainless steel in a boiling water reactor environment. The main conclusions are as follows:

a. The change of the random error of the corrosion potential has an important impact on the distribution of the crack growth rate. When the random error of the corrosion potential rises from 0.01VSHE to 0.03VSHE, the distribution of the corresponding crack growth rate changes from a normal distribution to a logarithmic positive State distribution. The random errors of other variables have no effect on the distribution of crack growth rate.

b. When all influencing variables follow a normal distribution, the distribution of crack growth rate also basically follows a normal distribution (except for the case where the corrosion potential has a higher standard deviation). Moreover, within the random error range of the influence variables selected in this chapter, the distribution of crack growth rate is basically 0.5 orders of magnitude.

c. The effect of temperature on crack growth rate is mainly affected by other environmental variables related to temperature. When other environmental variables are kept within a constant range, the temperature has almost no effect on the crack growth rate.

d. Finally, the sizes of the Standard Deviations (SDs) in the above variables relative to the means also have a profound impact on the distributions in the dependent variable. If the SDs are small, the distribution in the dependent variable becomes indistinguishable from a normal distribution. However, if the SDs are large, the distribution in the dependent variable in unequivocally lognormal.

Acknowledgment

The authors gratefully acknowledge the scholarship support of JS by the China Scholarship fund. They also gratefully acknowledge the support of this work by the University of California at Berkeley.

Data Availability

All data employed in this study are presented in the paper.

References

1. Nevdacha V, Yagozinskyy Y (2007) Dynamic strain ageing of deformed nitrogen-alloyed AISI 316 stainless steels. Corrosion Issues in Light Water Reactors: Stress Corrosion Cracking 8(51): 103-118.
2. Jain S, Ayello F, Beavers JA, Sridhar N (2012) Development of a probabilistic model for stress corrosion cracking of underground pipelines using Bayesian networks: A concept. In: 2012 9th International Pipeline Conference, American Society of Mechanical Engineers, Calgary, Alberta, Canada, pp. 615-625.
3. Jain S, Beavers JA, Ayello F, Sridhar N (2013) Probabilistic model for stress corrosion cracking of underground pipelines using Bayesian networks. Corrosion.
4. Priya C, Rao KB, Anoop MB, Lakshmanan N, Gopika V, et al. (2005) Probabilistic failure analysis of austenitic nuclear pipelines against stress corrosion cracking. I Mech Eng 219(7): 607-626.
5. Guedri A (2013) Reliability analysis of stainless-steel piping using a single stress corrosion cracking damage parameter. Int J Pres Ves Pip 111: 1-11.
6. Anoop MB, Balaji Rao K, Lakshmanan N (2008) Safety assessment of austenitic steel nuclear power plant pipelines against stress corrosion cracking in the presence of hybrid uncertainties. Int J Pres Ves Pip 85(4): 238-247.
7. Andresen PL, Ford FP (1994) Fundamental modeling of environmental cracking for improved design and lifetime evaluation in BWRs. Int J Pres Ves Pip 59(1-3): 61-70.
8. Macdonald DD, Urquidi-Macdonald M (1991) A coupled environment model for stress corrosion cracking in sensitized type 304 stainless steel in LWR environments. Corros Sci 32(1): 51-81.
9. Macdonald DD, Urquidi-Macdonald M (1991) An advanced coupled environment fracture model for predicting crack growth rates. Parkins Symposium on Fundamental Aspects of Stress Corrosion Cracking pp. 443-455.
10. Macdonald DD, Lu PC, UrquidiMacdonald M, Yeh TK (1996) Theoretical estimation of crack growth rates in type 304 stainless steel in boiling-water reactor coolant environments. Corrosion 52(10): 768-785.
11. Vankeerberghen M, Macdonald DD (2002) Predicting crack growth rate vs. temperature behaviour of type 304 stainless steel in dilute sulphuric acid solutions. Corros Sci 44(7): 1425-1441.
12. Lee SK, Lv P, Macdonald DD (2013) Customization of the CEFM for predicting stress corrosion cracking in lightly sensitized Al-Mg alloys in marine applications, J Solid State Electr 17: 2319-2332.
13. Maeng WY, Macdonald DD (2008) The effect of acetic acid on the stress corrosion cracking of 3.5NiCrMoV turbine steels in high temperature water. Corros Sci 50(8): 2239-2250.
14. Lee SK, Macdonald DD (2013) Stress corrosion cracking of alloy 22. In: 224th ECS Meeting, The Electrochemical Society, San Francisco, USA, pp. 1781-1781.
15. Shi J, Fekete B, Wang J, Macdonald DD (2018) Customization of the coupled environment fracture model for predicting stress corrosion cracking in Alloy 600 in PWR environment. Corrosion Science 139: 58-67.
16. Lee S, Macdonald DD (2013) Development of semi-elliptical surface cracks in lightly sensitized Al-Mg alloys. In: 224th ECS Meeting, The Electrochemical Society, San Francisco, USA, pp. 1780-1780.
17. Macdonald DD (1992) Viability of hydrogen water chemistry for protecting in-vessel components of boiling water-reactors. Corrosion 48(3): 194-205.
18. Manahan MP, Macdonald DD, Peterson AJ (1995) Determination of the fate of the current in the stress-corrosion cracking of sensitized type 304SS in high-temperature aqueous systems. Corros Sci 37: 189-208.

19. Gomez-Duran M, Macdonald DD (2003) Stress corrosion cracking of sensitized type 304 stainless steel in thiosulfate solution: I. Fate of the coupling current. Corros Sci 45(7): 1455-1471.

20. Gomez-Duran M, Macdonald DD (2006) Stress corrosion cracking of sensitized type 304 stainless steel in thiosulphate solution. II. Dynamics of fracture. Corros Sci 48(7): 1608-1622.

21. Liu S, Macdonald DD (2002) Fracture of AISI 4340 steel in concentrated sodium hydroxide solution. Corrosion 58(10): 835-845.

22. Engelhardt GR, Macdonald DD, Urquidi-Macdonald M (1999) Development of fast algorithms for estimating stress corrosion crack growth rate. Corros Sci 41(12): 2267-2302.

23. Andresen P (1993) Effects of temperature on crack growth rate in sensitized type 304 stainless steel and alloy 600. Corrosion 49(9): 714-725.

24. (2009) BWRVIP-226: BWRVIP vessel and internals project. Feasibility evaluation of BWR hydrogen injection for ECP reduction during startup. EPRI, Palo Alto, CA:1019074.

25. Shi J, Wang J, Macdonald DD (2014) Prediction of crack growth rate in type 304 stainless steel using artificial neural networks and the coupled environment fracture model. Corrosion Science 89: 69-80.

26. Shi J, Fekete B, Wang J, Macdonald DD (2018) Customization of the coupled environment fracture model for predicting stress corrosion cracking in Alloy 600 in PWR environment. Corrosion Science 139: 58-67.

27. Kwon HS, Wuensche A, Macdonald DD (2000) Effects of flow rate on crack growth in sensitized type 304 stainless steel in high-temperature aqueous solutions. Corrosion 56(5): 482-491.

28. Roychowdhury S, Kain V, Neogy S, Srivastava D, Dey GK, et al. (2012) Understanding the effect of nitrogen in austenitic stainless steel on the intergranular stress corrosion crack growth rate in high-temperature pure water. Acta Mater 60(2): 610-621.

29. (2000) Stress corrosion crack growth rate measurements on unsensitized type 304 stainless steel in 288 °C water. EPRI, Palo Alto, CA, TR-113489.

30. Macdonald DD (2023) The role of determinism in the prediction of corrosion damage. Corros Mater Degrad 4: 212-273.